Constant-Curvature Motion Planning Under Uncertainty with Applications in Image-Guided Medical Needle Steering

Ron Alterovitz[1], Michael Branicky[2], and Ken Goldberg[3]

[1] IEOR Department, University of California, Berkeley, ron@ieor.berkeley.edu
[2] EECS Department, Case Western Reserve University, mb@case.edu
[3] IEOR and EECS Departments, University of California, Berkeley, goldberg@berkeley.edu

Abstract: We consider a variant of nonholonomic motion planning for a Dubins car with no reversals, binary left/right steering, and uncertainty in motion direction. We apply our new motion planner to steerable needles, a new class of flexible bevel-tip medical needles that clinicians can steer through soft tissue to reach targets inaccessible to traditional stiff needles. Our method explicitly considers uncertainty in needle motion due to patient differences and the difficulty in predicting needle/tissue interaction: the planner computes optimal turning points to maximize the probability that the needle will reach the desired target. Given a medical image with segmented obstacles and target, our method formulates the planning problem as a Markov Decision Process (MDP) based on an efficient discretization of the state space, models motion uncertainty using probability distributions, and computes turning points to maximize the probability of success using infinite horizon Dynamic Programming (DP). This approach has three features particularly beneficial for medical planning problems. First, the planning formulation only requires parameters that can be directly extracted from images. Second, we can compute the optimal needle insertion point by examining the DP look-up table of optimal controls for every needle state. Third, intra-operative medical imaging can be combined with the pre-computed DP look-up table to permit optimal control of the needle in the operating room without requiring time-consuming intra-operative re-planning. We apply the method to generate motion plans for steerable needles to reach targets inaccessible to stiff needles and illustrate the importance of considering uncertainty during motion plan optimization.

1 Introduction

Advances in medical imaging such as x-ray fluoroscopy, ultrasound, and MRI are now providing physicians with real-time patient-specific information as they perform medical procedures such as biopsies to extract tissue samples, drug treatment injections for anesthesia, or radioactive seed implantations for

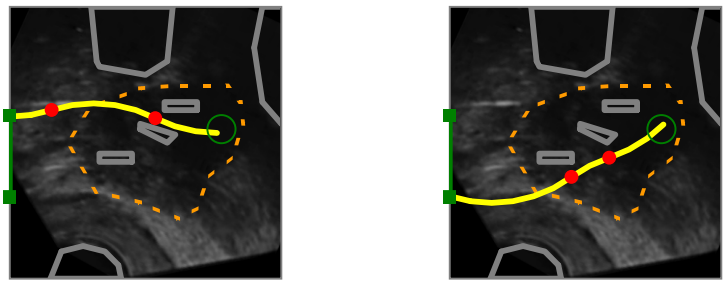

(a) Minimize path length
$P_s = 36.7\%$

(b) Maximize probability of success
$P_s = 73.7\%$

Fig. 1. In brachytherapy to treat prostate cancer, physicians implant radioactive seeds at precise locations inside the prostate under ultrasound image guidance. Brachytherapy is currently performed using rigid needles; here we consider steerable needles capable of obstacle avoidance. Our motion planner computes controls (insertions and direction changes, indicated by dots) to steer the needle from an insertion entry region (between the solid squares) to the target (open circle) inside soft tissue, without touching critical areas indicated by polygonal obstacles in the imaging plane. The motion of the needle is not known with certainty; the needle tip may be deflected during insertion due to tissue inhomogeneities or other unpredictable soft tissue interactions. We explicitly consider this uncertainty to generate motion plans to maximize the probability of success, P_s, the probability that the needle will reach the target without colliding with an obstacle or exiting the workspace boundary. Relative to minimizing path length, maximizing probability of success generates longer paths with greater clearance from obstacles, resulting in higher P_s.

brachytherapy cancer treatment. These diagnostic and therapeutic medical procedures require insertion of a needle to a specific location in soft tissue. We are developing motion planning algorithms for medical needle insertion procedures that can utilize the information obtained by real-time imaging to accurately reach desired locations.

We consider a new class of medical needles, composed of a flexible material and with a bevel-tip, that can be steered to targets in soft tissue that are inaccessible to traditional stiff needles [30, 31, 3, 4]. Steerable needles are controlled by 2 degrees of freedom actuated at the needle base: insertion distance and bevel direction. Webster et al. experimentally demonstrated that, under ideal conditions, a flexible bevel-tip needle cuts a path of constant curvature in the direction of the bevel and the needle shaft bends to follow the path cut by the bevel tip [30]. In a plane, this nonholonomic constraint based on bevel direction is equivalent to a Dubins car that cannot go straight; it can only steer its wheels far left or far right.

The steerable needle motion planning problem is to determine a sequence of controls (insertions and direction changes) so the needle tip reaches the specified target while avoiding obstacles and staying inside the workspace. Given a segmented medical image of the target, obstacles, and starting loca-

tion, the feasible workspace for motion planning is defined by the soft tissues through which the needle can be steered. Obstacles represent tissues that cannot be cut by the needle, such as bone, or sensitive tissues that should not be damaged, such as nerves or arteries. In this paper we consider motion plans in an imaging plane since the speed/resolution trade-off of 3D imaging modalities is generally poor for 3D real-time interventional applications. In future work, we will explore the natural extension of our planning approach to 3D as imaging modalities continue to improve.

Clinicians performing medical needle insertion procedures must consider uncertainty in the needle's motion through tissue due to patient differences and the difficulty in predicting needle/tissue interaction. These sources of uncertainty may result in deflections of the needle's orientation, which is a type of slip in the motion of a Dubins car. Real-time imaging in the operating room can measure the needle's current position and orientation, but this measurement by itself provides no information about the effect of future deflections during insertion. We develop a new motion planning approach for steering flexible needles through soft tissue that explicitly considers uncertainty: our method formulates the planning problem as a Markov Decision Process (MDP) based on an efficient discretization of the state space, models motion uncertainty using probability distributions, and computes optimal controls (within error due to discretization) using infinite horizon Dynamic Programming (DP).

To define optimality for a needle steering plan, we introduce a new objective for image-guided motion planning: maximizing probability of success. In the case of needle steering, the needle is controlled until it reaches the target (success) or until failure occurs, where failure is defined as hitting an obstacle, exiting the feasible workspace, or reaching a state in which it is impossible to prevent the former two outcomes. Since the motion response of the needle is not deterministic, success of the procedure can rarely be guaranteed. Our objective function value for a particular plan has physical meaning: it is the probability that the needle insertion will succeed assuming optimal control of the needle. In addition to this intuitive interpretation of the objective, our formulation has a secondary benefit: all data required for planning can be measured directly from imaging data without requiring tweaking of user-specified parameters. Rather than assigning costs to insertion distance, needle rotation, etc., which are difficult to estimate or quantify, our method only requires the probability distributions of the needle response to each feasible control, which can be estimated from previously obtained images.

Solving the MDP using DP has key benefits particularly relevant for medical planning problems where feedback is provided at regular time intervals using medical imaging or other sensor modalities. Like a well-constructed navigation field, the DP solver provides an optimal control for any state in the workspace. We use the DP look-up table to automatically optimize the needle insertion point. Integrated with intra-operative medical imaging, this DP look-up table can be used to optimally control the needle in the operating

room without requiring costly intra-operative re-planning. Hence, the planning solution can serve as a means of control under real-time medical imaging.

In Fig. 1, we apply our motion planner in simulation to prostate brachytherapy, a medical procedure in which physicians implant radioactive seeds at precise locations inside the prostate under ultrasound image guidance to treat prostate cancer. In this ultrasound image of the prostate (segmented by a dotted line), obstacles correspond to bones, the rectum, the bladder, the urethra, and previously implanted seeds. We compare the output of our new method to previous work on shortest path planning for steerable needles [4]. Our method improves the expected probability of success by over 30% compared to shortest path planning, illustrating the importance of explicitly considering uncertainty in needle motion.

2 Related Work

Nonholonomic motion planning has a long history in robotics and related fields [20, 21, 10, 23]. Past work has addressed deterministic curvature-constrained path planning where a mobile robot's path is, like a car, constrained by a minimum turning radius. Dubins showed that the optimal curvature-constrained trajectory in open space from a start pose to a target pose can be described from a discrete set of canonical trajectories composed of straight line segments and arcs of minimum radius of curvature [15]. Jacobs and Canny considered polygonal obstacles and constructed a configuration space for a set of canonical trajectories [18], and Agarwal et al. developed a fast algorithm for a shortest path inside a convex polygon [1]. For Reeds-Shepp cars with reverse, Laumond et el. developed a nonholonomic planner using recursive subdivision of collision-free paths generated by a lower-level geometric planner [22] and Bicchi et al. proposed a technique that provides the shortest path for circular unicycles [8]. Sellen developed a discrete state-space approach; his discrete representation of orientation using a unit circle inspired our discretization approach [27].

Our planning problem considers steerable needles currently under development that are subject to a *constant* magnitude turning radius rather than a *minimum* turning radius. Webster et al. showed experimentally that, under ideal conditions, steerable bevel-tip needles follow paths of constant curvature in the direction of the bevel tip [30], and that radius of curvature of the needle path is not significantly affected by insertion velocity [31].

Park et al. formulated the planning problem for steerable bevel-tip needles in stiff tissue as a nonholonomic kinematics problem based on a 3D extension of a unicycle model and used a diffusion-based motion planning algorithm to numerically compute a path [25]. Park's method searches for a feasible path in full 3D space using continuous control, but it does not consider obstacle avoidance or the uncertainty of the response of the needle to insertion or direction changes, both of which are emphasized in our method.

Past work has investigated needle insertion planning in situations where soft tissue deformations are significant and can be modeled. Our past work addressed planning optimal insertion location and insertion distance for rigid symmetric-tip needles to compensate for 2D tissue deformations [5, 6]. Past work has also addressed steering slightly flexible symmetric-tip needles by translating and orienting the needle base to explicitly cause tissue deformations that will guide the needle around point obstacles with oval-shaped potential fields [14]. Glozman and Shoham also address symmetric-tip needles and approximate the tissue using springs [17]. We previously developed a different 2D planner for bevel-tip needles to explicitly compensate for the effects of tissue deformation by combining finite element simulation with numeric optimization [3]. This previous approach assumed that bevel direction can only be set once prior to insertion and employed local optimization that can fail to find a globally optimal solution in the presence of obstacles.

In preliminary work, we proposed an MDP formulation for needle steering [4] to find a stochastic shortest path from a start position to a target, subject to user-specified "cost" parameters for direction changes, insertion distance, and obstacle collisions. However, the formulation was not targeted at image-guided procedures, did not include insertion point optimization, and optimized an objective function that has no physical meaning. In this paper, we develop a 2D motion planning approach for image-guided needle steering that explicitly considers motion uncertainty to maximize the probability of success based on parameters that can be extracted from medical imaging without requiring user-specified "cost" parameters that may be difficult to determine.

MDP's are ideally suited for medical planning problems because of the variance in characteristics between patients and the necessity for clinicians to make decisions at discrete time intervals based on limited known information. In the context of medical procedure planning, MDP's have been developed to assist in timing decisions for liver transplants [2], discharge of severe sepsis cases [19], and start dates for HIV drug cocktail treatment [28].

Integrating motion planning with intra-operative medical imaging requires real-time localization of the needle in the images. Methods are available for this purpose for a variety of imaging modalities [11, 12]. X-ray fluoroscopy, a relatively low-cost imaging modality capable of obtaining images at regular discrete time intervals, is ideally suited for our application because it generates 2D projection images from which the needle can be cleanly segmented [11].

Medical needle insertion procedures may also benefit from the more precise control of needle position and velocity made possible through robotic surgical assistants [29]. Dedicated hardware for needle insertion is being developed for stereotactic neurosurgery [24], MR compatible surgical assistance [9, 13], and prostate biopsy and therapeutic interventions [16, 26].

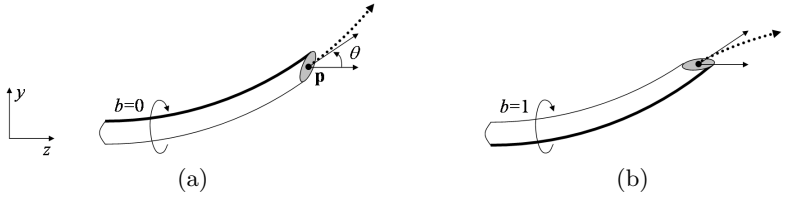

Fig. 2. The state of a steerable needle during insertion is characterized by tip position $\mathbf{p}$, tip orientation angle θ, and bevel direction b (a). Rotating the needle about its base changes the bevel direction but does not affect needle position (b). The needle will cut soft tissue along an arc (dotted vector) based on bevel direction.

3 Motion Planning Method

3.1 Problem Definition

Steerable bevel-tip needles are controlled by 2 degrees of freedom actuated at the needle base: insertion distance and rotation angle about the needle axis. Insertion pushes the needle deeper into the tissue, while rotation re-orients the bevel at the needle tip. For a sufficiently flexible needle, Webster et al. experimentally demonstrated that rotating the needle base will change the bevel direction without changing the needle's position in the tissue [30]. In the plane, the needle base can be rotated 180° about the insertion axis at the base so the bevel points in either the bevel-left or bevel-right direction. When inserted, the asymmetric force applied by the bevel causes the needle to bend and follow a curved path through the tissue [30]. Under ideal conditions, the curve will have a constant radius of curvature r, which is a property of the needle and tissue. We assume the tissue is stiff relative to the needle and that the needle is thin, sharp, and low-friction so the tissue does not significantly deform. While the needle can be partially retracted and re-inserted, the needle is likely to follow the path in the tissue cut by the needle prior to retraction. Hence, we only consider insertion, not retraction, of the needle in this paper.

We define the workspace as a 2D rectangle of depth z_{max} and height y_{max}. We do not consider motion by the needle out of the imaging plane. Obstacles in the workspace are defined by (possibly nonconvex) polygons. The obstacles can be expanded using a Minkowski sum to specify a minimum clearance [23]. The target region is defined by a circle with center point $\mathbf{t}$ and radius r_t.

As shown in Fig. 2, the state w of the needle during insertion is fully characterized by the needle tip's position $\mathbf{p} = (p_y, p_z)$, orientation angle θ, and bevel direction b, where b is either bevel-left (b=0) or bevel-right (b=1).

We assume imaging occurs at discrete time intervals and the motion planner obtains needle tip position and orientation information only at these times. Between images, we assume the needle moves at constant velocity and is inserted a distance δ. In our model, direction changes can only occur at discrete *decision points* separated by the insertion distance δ. One of two controls, or

actions, u can be selected at any decision point: insert the needle a distance δ ($u = 0$), or change direction and insert a distance δ ($u = 1$).

During insertion, the needle tip orientation may be deflected by inhomogeneous tissue, small anatomical structures not visible in medical images, or local tissue displacements. Additional deflection may occur during direction changes due to stiffness along the needle shaft. These deflections are due to an unknown aspect of the tissue structure or needle/tissue interaction, not errors in measurement of the needle's orientation, and can be considered a type of noise parameter in the plane. We model uncertainty in needle motion due to such deflections using probability distributions. The orientation angle θ may be deflected by some angle β, which we model as normally distributed with mean 0 and standard deviations σ_i for insertion ($u = 0$) and σ_r for direction changes followed by insertion ($u = 1$). Since σ_i and σ_r are properties of the needle and tissue, we plan in future work to automatically estimate these parameters by retrospectively analyzing images of needle insertion.

The goal of motion planning is to compute an optimal control u for every state w in the workspace to maximize the probability of success P_s. We define $P_s(w)$ to be the probability of success given that the needle is currently in state w. If the position of state w is inside the target, $P_s(w) = 1$. If the position of state w is inside an obstacle, $P_s(w) = 0$. Given a control u for some other state w, the probability of success will depend on the response of the needle to the control (the next state) and the probability of success for that next state. The expected probability of success is $P_s(w) = E[P_s(v)|w, u]$, where the expectation is over v, a random variable for the next state. The goal of motion planning is to compute an optimal control u for every state w:

$$P_s(w) = \max_u \{E[P_s(v)|w, u]\} . \tag{1}$$

3.2 Problem Formulation

To evaluate Eq. 1, we approximate needle state $w = \{\mathbf{p}, \theta, b\}$ using a discrete representation. To make this approach tractable, we must round $\mathbf{p}$ and θ without generating an unwieldy number of states while simultaneously bounding error due to discretization. We describe our approximation approach, which results in N discrete states, in Sec. 3.3.

For N discrete states, the motion planning problem is to determine the optimal control u_i for each state $i = 1, \ldots, N$. We re-write Eq. 1 using the discrete approximation and expand the expected value to a summation:

$$P_s(x_i) = \max_{u_i} \left\{ \sum_{j=1}^{N} P_{ij}(u_i) P_s(x_j) \right\} , \tag{2}$$

where $P_{ij}(u_i)$ is the probability of entering state x_j after executing control u_i at current state x_i.

We observe that the needle steering motion planning problem is a type of MDP. In particular, Eq. 2 has the form of the Bellman equation for a stochastic shortest path problem [7]:

$$J^*(x_i) = \max_{u_i} \sum_{j=1}^{N} P_{ij}(u_i) \left(g(x_i, u_i, x_j) + J^*(x_j) \right). \tag{3}$$

where $g(x_i, u_i, x_j)$ is a "reward" for transitioning from state x_i to x_j after control u_i. In our case, $g(x_i, u_i, x_j) = 0$ for all x_i, u_i, and x_j, and $J^*(x_i) = P_s(x_i)$. Stochastic shortest path problems of this form can be optimally solved using infinite horizon DP, as we describe in Sec. 3.4.

3.3 State Space Discretization

Our discretization of the planar workspace is based on a grid of points with a spacing Δ horizontally and vertically. We approximate a point $\mathbf{p} = (p_y, p_z)$ by rounding to the nearest point $\mathbf{q} = (q_y, q_z)$ on the grid. For a rectangular workspace bounded by depth z_{max} and height y_{max}, this results in $N_s = \left\lfloor z_{max} y_{max} / \Delta^2 \right\rfloor$ position states aligned at the origin.

Rather than directly approximating θ by rounding, which would incur a cumulative error with every transition, we take advantage of discrete insertion distances δ. We define a *control circle* of radius r, the radius of curvature of the needle. Each point $\mathbf{c}$ on the control circle represents an orientation θ of the needle, where θ is the angle of the tangent of the circle at $\mathbf{c}$ with respect to the z-axis. The needle will trace an arc of length δ along the control circle in a counter-clockwise direction for $b = 0$ and in the clockwise direction for $b = 1$. Direction changes correspond to rotating the point $\mathbf{c}$ by 180° about the control circle origin and tracing subsequent insertions in the opposite direction, as shown in Fig. 3(a). Since the needle traces arcs of length δ, we divide the control circle into N_c arcs of length $\delta = 2\pi r / N_c$. The endpoints of the arcs generate a set of N_c control circle points, each representing a discrete orientation state, as shown in Fig. 3(b). We require that N_c is a multiple of 4 to facilitate the orientation state change after a direction change.

At each position on the Δ grid, the needle may be in any of the N_c orientation states. To define transitions for each orientation state, we overlay the control circle on a regular grid of spacing Δ and round the positions of the control circle points to the nearest grid point, as shown in Fig. 3(c). The displacements between rounded control circle points encode the transitions of the needle tip. This discretization results in 0 discretization error in orientation when the needle is controlled at δ intervals.

Using this discretization, a needle state $w = \{\mathbf{p}, \theta, b\}$ can be approximated as a discrete state $s = \{\mathbf{q}, \Theta, b\}$, where $\mathbf{q} = (q_y, q_z)$ is the discrete point closest to $\mathbf{p}$ on the Δ-density grid and Θ is the integer index of the discrete control circle point with tangent angle closest to θ. The total number of discrete states is $N = 2N_sN_c$.

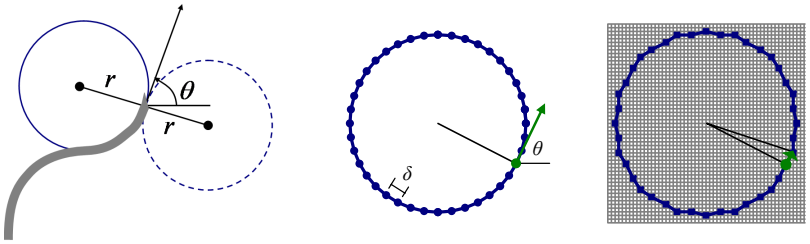

(a) Needle tracing control circle (b) Control circle (c) Rounded control circle

Fig. 3. A needle in the bevel-left direction with orientation θ is tracing the solid control circle with radius r (a). A direction change would result in tracing the dotted circle. The control circle is divided into $N_c = 40$ discrete arcs of length δ (b). The control circle points are rounded to the nearest point on the Δ-density grid, and transitions for insertion of distance δ are defined by the vectors between rounded control circle points (c).

Deterministic paths designated using this discrete representation of state will incur error due to discretization, but the error is bounded. At any decision point, the position error due to rounding to the Δ workspace grid is $E_0 = \Delta\sqrt{2}/2$. When the bevel direction is changed, a position error is also incurred because the distance in centers of the original control circle and the center of the control circle after the direction change will be in the range $2r \pm \Delta\sqrt{2}$. Hence, for a needle path with h direction changes, the final orientation is precise but the error in position is bounded above by $E_h = h\Delta\sqrt{2} + \Delta\sqrt{2}/2$.

Due to motion uncertainty, actual needle paths will not always exactly trace the control circle. The deflection angle β defined in Sec. 3.1 must also be approximated as discrete. We define discrete transitions from a state x_i, each separated by an angle of deflection of $\alpha = 360°/N_c$, and store the transition probability in $P_{ij}(u)$. In this paper, we model β using a normal distribution with mean 0 and standard deviation σ_i or σ_r, and compute the probability for each discrete transition by integrating the corresponding area under the normal curve, as shown in Fig. 4. We set the number of discrete transitions N_{p_i} such that the areas on the left and right tails of the normal distribution sum to less than 1%. The left and right tail probabilites are added to the left-most and right-most transitions, respectively.

Certain states and transitions must be handled as special cases. States inside the target region and states inside obstacles are absorbing states. If the transition arc from feasible state x_i exits the workspace or intersects an edge of a polygonal obstacle, a transition to an obstacle state is used.

3.4 Optimization Using Infinite Horizon Dynamic Programming

Infinite horizon dynamic programming is a type of dynamic programming in which there is no finite time horizon [7]. For stationary problems, this

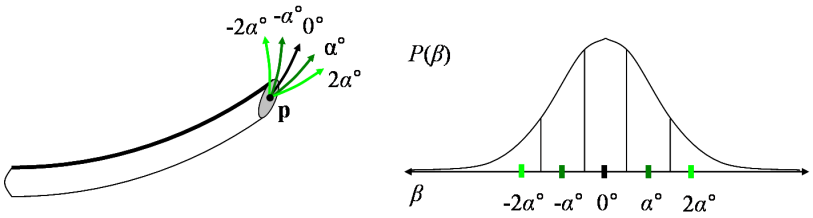

Fig. 4. When the needle is inserted, the insertion angle θ may be deflected by some angle β. We model the probability distribution of β using a normal distribution with mean 0 and standard deviation σ_i for insertion or σ_r for direction change. For a discrete sample of deflections ($\beta = \{-2\alpha, -\alpha, 0, \alpha, 2\alpha\}$), we obtain the probability of each deflection by integrating the corresponding area under the normal curve.

implies that the optimal control at each state is purely a function of the state without explicit dependence on time. In the case of needle steering, once a state transition is made, the next control is computed based on the current position, orientation, and bevel direction without explicit dependence on past controls.

To solve the infinite horizon DP problem defined by the Bellman Eq. 3, we use the value iteration algorithm [7], which iteratively updates $P_s(x_i)$ for each state i by evaluating Eq. 2. This generates a DP look-up table containing the optimal control u_i and the probability of success $P_s(x_i)$ for $i = 1, \ldots, N$.

Termination of the algorithm is guaranteed in N iterations if the transition probability graph corresponding to some optimal stationary policy is acyclic [7]. Violation of this requirement will be rare in motion planning since it implies that an optimal control sequence results in a path that, with probability greater than 0, loops and passes through the same point at the same orientation more than once. Each iteration requires matrix-vector multiplication. To improve performance, we take advantage of the sparsity of the matrices $P_{ij}(u)$ for $u = 0$ and $u = 1$. Although $P_{ij}(u)$ has N^2 entries, each row of $P_{ij}(u)$ has only k nonzero entries, where $k << N$ since the needle will only transition to a state j in the spatial vicinity of state i. Hence, $P_{ij}(u)$ has at most kN nonzero entries. By only accessing nonzero entries of $P_{ij}(u)$ during computation, each iteration of the value iteration algorithm requires only $O(kN)$ rather than $O(N^2)$ time and memory. Thus, the total algorithm's complexity is $O(kN^2)$. To further improve performance, we terminate value iteration when the maximum change ϵ over all states is less than 10^{-3}, which in our test cases occurred in far fewer than N iterations, as described in Sec. 4.

4 Computational Results

We implemented the motion planner in C++ and tested it on a 2.21GHz Athlon 64 PC. In Fig. 1, we set the needle radius of curvature $r = 5.0$, defined

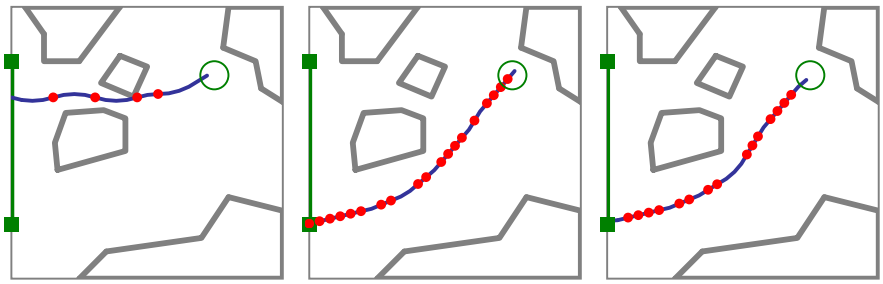

(a) Shortest path (Deterministic)

(b) Maximize P_s $\sigma_i = 10^\circ$, $\sigma_r = 10^\circ$ $P_s = 76.95\%$

(c) Maximize P_s $\sigma_i = 20^\circ$, $\sigma_r = 20^\circ$ $P_s = 29.01\%$

Fig. 5. As in Fig. 1, optimal plans maximizing the probability of success P_s illustrate the importance of considering uncertainty in needle motion. The shortest path plan passes through a narrow gap between obstacles (a). Since maximizing P_s explicitly considers uncertainty, the optimal expected path has greater clearance from obstacles, decreasing the probability that large deflections will cause failure to reach the target. Here we consider medium (b) and large (c) variance in tip deflections for a needle with smaller radius of curvature than in Fig. 1.

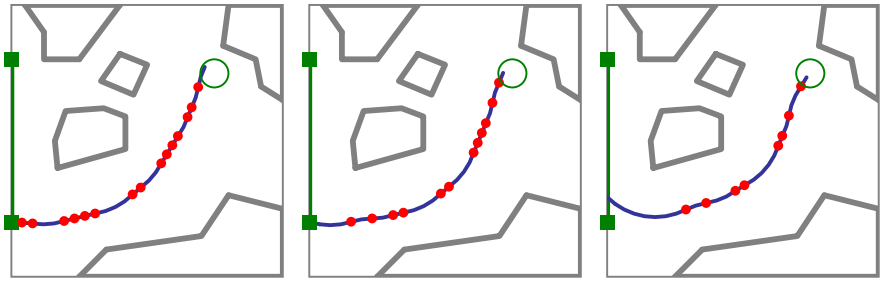

(a) $\sigma_i = 5^\circ$, $\sigma_r = 5^\circ$, $P_s = 98.98\%$

(b) $\sigma_i = 5^\circ$, $\sigma_r = 10^\circ$, $P_s = 92.87\%$

(c) $\sigma_i = 5^\circ$, $\sigma_r = 20^\circ$, $P_s = 73.00\%$

Fig. 6. Optimal plans demonstrate the importance of considering uncertainty in needle motion, where σ_i and σ_r are the standard deviations of needle tip deflections that can occur during insertion and direction changes, respectively. For higher σ_r relative to σ_i, the optimal plan includes fewer direction changes. Needle motion uncertainty at locations of direction changes may be substantially higher than uncertainty during insertion due to transverse stiffness of the needle.

the workspace by $z_{max} = y_{max} = 10$, and used discretization parameters $N_c = 40$, $\Delta = 0.1$, and $\delta = 0.785$. The resulting DP problem contained $N =$ 800,000 states. In all further examples, we set $r = 2.5$, $z_{max} = y_{max} = 10$, $N_c = 40$, $\Delta = 0.1$, and $\delta = 0.393$, resulting in $N = 800{,}000$ states.

Optimal plans and probability of success P_s depend on the level of uncertainty in needle motion. As shown in Figs. 1 and 5, explicitly considering

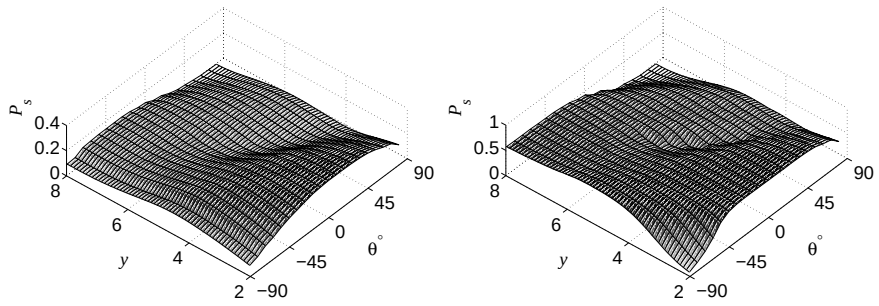

(a) Optimization surface for Fig. 5(c) (b) Optimization surface for Fig. 6(c)

Fig. 7. The optimal needle insertion location y, angle θ, and bevel direction b are found by scanning the DP look-up table for the feasible start state with maximal P_s. Here we plot optimization surfaces for $b = 0$. The low regions correspond to states from which the needle has high probability of colliding with an obstacle or exiting the workspace, and the high regions correspond to better start states.

the variance of needle motion significantly affects the optimal plan relative to shortest path plan generated under the assumption of deterministic motion. We also vary the variance during direction changes independently from the variance during insertions without direction changes. Optimal plans and probability of success P_s are highly sensitive to the level of uncertainty in needle motion due to direction changes. As shown in Fig. 6, the number of direction changes decreases as the variance during direction changes increases.

By examining the DP look-up table, we can optimize the initial insertion location, orientation, and bevel direction, as shown in Figs. 1, 5, and 6. In these examples, the set of feasible start states was defined as a subset of all states on the left edge of the workspace. By linearly scanning the DP look-up table, the method identifies the bevel direction b, insertion point (height y on the left edge of the workspace), and starting orientation angle θ (which varies from -90° to 90°) that maximizes probability of success, as shown in Fig. 7.

Integrating intra-operative medical imaging with the pre-computed DP look-up table could permit optimal control of the needle in the operating room without requiring costly intra-operative re-planning. We demonstrate the potential of this approach using simulation of needle deflections based on normal distributions with mean 0 and standard deviations $\sigma_i = 5^\circ$ and $\sigma_r = 20^\circ$ in Fig. 8. After each insertion distance δ, we assume the needle tip is localized in the image. Based on the DP look-up table, the needle is either inserted or the bevel direction is changed. The effect of uncertainty can be seen as deflections in the path, i.e., locations where the tangent of the path abruptly changes. Since $\sigma_r > \sigma_i$, deflections are more likely to occur at points of direction change. In practice, clinicians could monitor P_s, insertion length, and self-intersection while performing needle insertion.

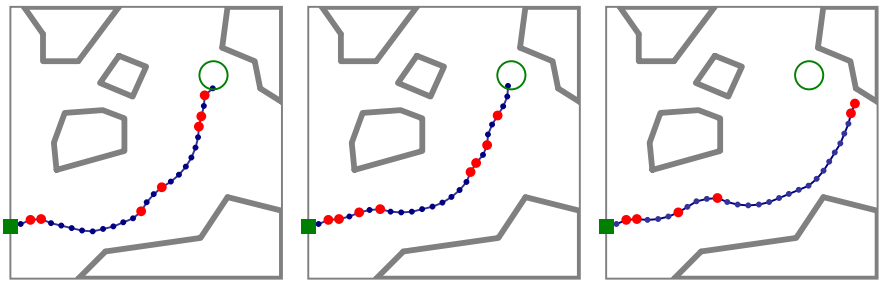

(a) (b) (c)

Fig. 8. Three simulated image-guided needle insertion procedures from a fixed starting point with needle motion uncertainty standard deviations of $\sigma_i = 5^\circ$ during insertion and $\sigma_r = 20^\circ$ during direction changes. After each insertion distance δ, we assume the needle tip is localized in the image and identified using a dot. Based on the DP look-up table, the needle is either inserted (small dots) or a direction change is made (larger dots). The effect of uncertainty can be seen as deflections in the path, i.e., locations where the tangent of the path abruptly changes. Since $\sigma_r > \sigma_i$, deflections are more likely to occur at points of direction change. In all cases, $P_s = 72.35\%$ at the initial state. In (c), multiple deflections and the nonholonomic constraint on needle motion prevent the needle from reaching the target.

As defined in Sec. 3.4, the computational complexity of the motion planner is $O(kN^2)$. Fewer than 300 iterations were required for each example, with fewer iterations required for smaller σ_i and σ_r. In all examples, the number of transitions per state $k \leq 25$. Computation time to solve the MDP for the examples ranged from 67 sec to 110 sec on a 2.21GHz AMD Athlon 64 PC, with higher computation times required for problems with greater variance, due to the increased number of transitions from each state. As computation only needs to be performed at the pre-procedure stage, we believe this computation time is reasonable for the intended applications. Intra-operative computation time is effectively instantaneous since only a memory access to the DP look-up table is required to retrieve the optimal control after the needle has been localized in imaging.

5 Conclusion and Future Work

We developed a new motion planning approach for steering flexible needles through soft tissue that explicitly considers uncertainty: the planner computes optimal controls to maximize the probability that the needle will reach the desired target. Motion planning for steerable needles, which can be controlled by 2 degrees of freedom at the needle base (bevel direction and insertion distance), is a variant of nonholonomic planning for a Dubins car with no reversals, binary left/right steering, and uncertainty in motion direction.

Given a medical image with segmented obstacles and target, our method formulates the planning problem as a Markov Decision Process (MDP) based on an efficient discretization of the state space, models motion uncertainty using probability distributions, and computes controls to maximize the probability of success using infinite horizon DP. We implemented the motion planner and ran test problems of 800,000 states on a 2.21GHz Athlon 64 PC. The method generated motion plans for steerable needles to reach targets inaccessible to stiff needles and illustrated the importance of considering uncertainty in needle motion, as shown in Figs. 1, 5, and 6.

Our approach has key features particularly beneficial for medical planning problems. First, the planning formulation only requires parameters that can be directly extracted from images (the variance of needle orientation after insertion with or without direction change). Second, we can locate the optimal needle insertion point by examining the DP look-up table of optimal controls for every needle state, as demonstrated in Fig. 7. Third, intra-operative medical imaging can be combined with the pre-computed DP look-up table to permit optimal control of the needle in the operating room without requiring time-consuming intra-operative re-planning, as shown in Fig. 8.

In future work, we plan to extend the motion planner to 3D. Although the mathematical formulation can be naturally extended, substantial effort will be required to specify 3D state transitions and improve solving methods to handle the larger state space. We also plan to develop automated methods to estimate curvature and variance properties from images and explore the inclusion of multiple tissue types in the workspace with different needle/tissue interaction properties.

Our motion planner has implications outside the needle steering domain. We can directly extend the method to motion planning problems with a bounded number of discrete turning radii where current position and orientation can be measured but future motion response to controls is uncertain. For example, mobile robots subject to motion uncertainty with similar properties can receive periodic "imaging" updates from GPS or satellite images. Optimization of "insertion location" could apply to automated guided vehicles in a factory setting, where one machine is fixed but a second machine can be placed to maximize the probability that the vehicle will not collide with other objects on the factory floor. By identifying a relationship between needle steering and infinite horizon DP, we developed a motion planner capable of rigorously computing plans that are optimal in the presence of uncertainty.

Acknowledgment

This work was supported in part by the NIH under grant R21 EB003452 and a NSF Graduate Research Fellowship to Ron Alterovitz. We thank Andrew Lim and A. Frank van der Stappen for their suggestions, and clinicians Leonard Shlain of CPMC and I-Chow Hsu and Jean Pouliot of UCSF for their input

on medical aspects of this work. We particularly thank Allison Okamura, Greg Chirikjian, Noah Cowan, and Robert Webster, our collaborators at JHU studying steerable needles.

References

1. P. K. Agarwal, T. Biedl, S. Lazard, S. Robbins, S. Suri, and S. Whitesides. Curvature-constrained shortest paths in a convex polygon. *SIAM J. Comput.*, 31(6):1814–1851, 2002.
2. O. Alagoz, L. M. Maillart, A. J. Schaefer, and M. Roberts. The optimal timing of living-donor liver transplantation. *Management Science*, 50(10):1420–1430, 2005.
3. R. Alterovitz, K. Goldberg, and A. Okamura. Planning for steerable bevel-tip needle insertion through 2D soft tissue with obstacles. In *Proc. IEEE Int. Conf. on Robotics and Automation*, pages 1652–1657, Apr. 2005.
4. R. Alterovitz, A. Lim, K. Goldberg, G. S. Chirikjian, and A. M. Okamura. Steering flexible needles under Markov motion uncertainty. In *Proc. IEEE/RSJ Int. Conf. on Intelligent Robots and Systems*, pages 120–125, Aug. 2005.
5. R. Alterovitz, J. Pouliot, R. Taschereau, I.-C. Hsu, and K. Goldberg. Needle insertion and radioactive seed implantation in human tissues: Simulation and sensitivity analysis. In *Proc. IEEE Int. Conf. on Robotics and Automation*, volume 2, pages 1793–1799, Sept. 2003.
6. R. Alterovitz, J. Pouliot, R. Taschereau, I.-C. Hsu, and K. Goldberg. Sensorless planning for medical needle insertion procedures. In *Proc. IEEE/RSJ Int. Conf. on Intelligent Robots and Systems*, volume 3, pages 3337–3343, Oct. 2003.
7. D. P. Bertsekas. *Dynamic Programming and Optimal Control*. Athena Scientific, Belmont, MA, 2nd edition, 2000.
8. A. Bicchi, G. Casalino, and C. Santilli. Planning shortest bounded-curvature paths for a class of nonholonomic vehicles among obstacles. In *Proc. IEEE Int. Conf. on Robotics and Automation*, pages 1349–1354, 1995.
9. K. Chinzei, N. Hata, F. A. Jolesz, and R. Kikinis. MR compatible surgical assist robot: System integration and preliminary feasibility study. In *Medical Image Computing and Computer Assisted Intervention*, pages 921–930, Oct. 2000.
10. H. Choset, K. M. Lynch, S. Hutchinson, G. Kantor, W. Burgard, L. E. Kavraki, and S. Thrun. *Principles of Robot Motion: Theory, Algorithms, and Implementations*. MIT Press, 2005.
11. K. Cleary, L. Ibanez, N. Navab, D. Stoianovici, A. Patriciu, and G. Corral. Segmentation of surgical needles for fluoroscopy servoing using the insight software toolkit (itk). In *Proc. Int. Conf. of the IEEE Engineering In Medicine and Biology Society*, pages 698–701, 2003.
12. S. P. DiMaio, D. F. Kacher, R. E. Ellis, G. Fichtinger, N. Hata, G. P. Zientara, L. P. Panych, R. Kikinis, and F. A. Jolesz. Needle artifact localization in 3T MR images. In J. D. Westwood et al., editors, *Medicine Meets Virtual Reality 14*, pages 120–125. IOS Press, Jan. 2006.
13. S. P. DiMaio, S. Pieper, K. Chinzei, N. Hata, E. Balogh, G. Fichtinger, C. M. Tempany, and R. Kikinis. Robot-assisted needle placement in open-MRI: System architecture, integration and validation. In J. D. Westwood et al., editors, *Medicine Meets Virtual Reality 14*, pages 126–131. IOS Press, Jan. 2006.

14. S. P. DiMaio and S. E. Salcudean. Needle steering and model-based trajectory planning. In *Medical Image Computing and Computer Assisted Intervention*, pages 33–40, 2003.
15. L. Dubins. On curves of minimal length with a constraint on average curvature and with prescribed initial and terminal positions and tangents. *American J. of Mathematics*, 79:497–516, 1957.
16. G. Fichtinger, T. L. DeWeese, A. Patriciu, A. Tanacs, D. Mazilu, J. H. Anderson, K. Masamune, R. H. Taylor, and D. Stoianovici. System for robotically assisted prostate biopsy and therapy with intraoperative CT guidance. *Academic Radiology*, 9(1):60–74, 2002.
17. D. Glozman and M. Shoham. Flexible needle steering and optimal trajectory planning for percutaneous therapies. In *Medical Image Computing and Computer Assisted Intervention*, Sept. 2004.
18. P. Jacobs and J. Canny. Planning smooth paths for mobile robots. In *Proc. IEEE Int. Conf. on Robotics and Automation*, pages 2–7, May 1989.
19. J. Kreke, A. J. Schaefer, M. Roberts, and M. Bailey. Optimizing testing and discharge decisions in the management of severe sepsis. In *Annual Meeting of INFORMS*, Nov. 2005.
20. J.-C. Latombe. *Robot Motion Planning*. Kluwer Academic Pub., 1991.
21. J.-C. Latombe. Motion planning: A journey of robots, molecules, digital actors, and other artifacts. *Int. J. of Robotics Research*, 18(11):1119–1128, Nov. 1999.
22. J.-P. Laumond, P. E. Jacobs, M. Taïx, and R. M. Murray. A motion planner for nonholonomic mobile robots. *IEEE Trans. on Robotics and Automation*, 10(5):577 – 593, Oct. 1994.
23. S. M. LaValle. *Planning Algorithms*. Cambridge University Press, 2006.
24. K. Masamune, L. Ji, M. Suzuki, T. Dohi, H. Iseki, and K. Takakura. A newly developed stereotactic robot with detachable drive for neurosurgery. In *Medical Image Computing and Computer Assisted Intervention*, 1998.
25. W. Park, J. S. Kim, Y. Zhou, N. J. Cowan, A. M. Okamura, and G. S. Chirikjian. Diffusion-based motion planning for a nonholonomic flexible needle model. In *Proc. IEEE Int. Conf. on Robotics and Automation*, pages 4611–4616, Apr. 2005.
26. C. Schneider, A. M. Okamura, and G. Fichtinger. A robotic system for transrectal needle insertion into the prostate with integrated ultrasound. In *Proc. IEEE Int. Conf. on Robotics and Automation*, pages 2085–2091, May 2004.
27. J. Sellen. Approximation and decision algorithms for curvature-constrained path planning: A state-space approach. In P. K. Agarwal, L. E. Kavraki, and M. T. Mason, editors, *Workshop on the Algorithmic Foundations of Robotics*, pages 59–67. AK Peters, Ltd., Houston, 1998.
28. S. Shechter, A. J. Schaefer, S. Braithwaite, M. Roberts, and M. Bailey. The optimal time to initiate HIV therapy. In *Annual Meeting of INFORMS*, Nov. 2005.
29. R. H. Taylor and D. Stoianovici. Medical robotics in computer-integrated surgery. *IEEE Trans. on Robotics and Automation*, 19(5):765–781, Oct. 2003.
30. R. J. Webster III, N. J. Cowan, G. Chirikjian, and A. M. Okamura. Nonholonomic modeling of needle steering. In *Proc. 9th Int. Symp. on Experimental Robotics*, June 2004.
31. R. J. Webster III, J. Memisevic, and A. M. Okamura. Design considerations for robotic needle steering. In *Proc. IEEE Int. Conf. on Robotics and Automation*, pages 3599–3605, Apr. 2005.